

How to evaluate the adiabatic condition for quantum annealing in an experiment

Yuichiro Mori,^{1,*} Shiro Kawabata,^{1,2,†} and Yuichiro Matsuzaki^{1,2,‡}

¹*Research Center for Emerging Computing Technologies (RCECT),
National Institute of Advanced Industrial Science and Technology (AIST),
1-1-1, Umezono, Tsukuba, Ibaraki 305-8568, Japan*

²*NEC-AIST Quantum Technology Cooperative Research Laboratory,
National Institute of Advanced Industrial Science and Technology (AIST), Tsukuba, Ibaraki 305-8568, Japan*

(Dated: August 5, 2022)

We propose an experimental method to evaluate the adiabatic condition during quantum annealing. The adiabatic condition is composed of the transition matrix element and the energy gap, and our method simultaneously provides information about these without diagonalizing the Hamiltonian. The key idea is to measure a power spectrum of a time domain signal by adding an oscillating field during quantum annealing, and we can estimate the values of transition matrix element and energy gap from the measurement output. Our results provide a powerful experimental tool to analyze the performance of quantum annealing, which will be essential for solving practical combinatorial optimization problems.

I. INTRODUCTION

The adiabatic theorem is one of the central results in quantum mechanics. It was first proposed by Ehrenfest [1] in 1916. Born and Fock proved a modern version of the theorem in 1928. The statement of the theorem is as follows. If we prepare an initial state in a ground state of the Hamiltonian, the state remains in the ground state of the Hamiltonian as long as the change in the Hamiltonian is sufficiently slow. Since the 1928 proof, there have been many subsequent studies, including more rigorous formulations [2, 3], or even extensions to open systems [4].

One of the essential applications of this theorem is quantum annealing (QA). The first proposal was made by Apolloni et al. in 1989 [5]. This original idea focused on improving simulated annealing using the quantum effects of tunneling. An alternative proposal was made [6, 7] where the Hamiltonian changes with time. In this proposal, we prepare a ground state of the transverse field Hamiltonian, and gradually change the Hamiltonian into the target Hamiltonian. The adiabatic theorem guarantees that, as long as the change in the Hamiltonian is sufficiently slow, the state after the evolution is the ground state of the problem Hamiltonian.

Nowadays, quantum annealing has been intensively studied from a variety of view points. In fact, there are studies in terms of computational speed [8–10], implementation methods [11, 12], and algorithms [13–15]. Commercial use of quantum annealing machines has also started by D-Wave, and accordingly, proposals for their use in research and applications in various fields are arising. Some of these include examples in quantum chemistry [16, 17], machine learning [18, 19], or even high-energy physics [20].

One of the problems of QA is that there are no known efficient methods to check whether the adiabaticity is satisfied. In principle, if we can diagonalize the Hamiltonian, we can use the following conditions as sufficient conditions to satisfy the adiabaticity [21–24]

$$\frac{|\langle m(t)|\dot{\mathcal{H}}(t)|0(t)\rangle|}{|E_m(t) - E_0(t)|^2} \ll 1, \quad (1)$$

for all t and m , where $|m(t)\rangle$ ($|0(t)\rangle$) denotes the m -th excited (ground) state, $\mathcal{H}(t)$ and $E_m(t)$ ($E_0(t)$) denotes the eigenenergy of the m -th excited (ground) state. (See Appendix A). However, when we perform QA to solve practical problems, we cannot diagonalize the Hamiltonian by a classical computer, and so we cannot directly use the above adiabatic conditions to check whether the dynamics are adiabatic. There are proposed methods to experimentally measure the energy gap [15, 25, 26], which corresponds to the denominator of the equation, Eq. (1). However, to our best knowledge, no studies have been performed to measure the numerator of the adiabatic condition (1), the size of the transition matrix element of the time derivative of the Hamiltonian.

In this paper, we propose a method to simultaneously measure the adiabatic condition's numerator and denominator. The key idea is to use oscillating field in the middle of quantum annealing, which induces a Rabi oscillation between the ground and excited state. By performing Fourier transformation of a time domain signal, we obtain a power spectrum and extract information from the obtained data. From these processes, we can estimate the values of the numerator and denominator of the adiabatic condition.

Our paper is organized as follows. In sec. III, we introduce our method to simultaneously measure the values of the transition matrix element and the energy gap based on an analytical calculation using some approximations. In sec. IV, to quantify the performance of our method in realistic cases, we perform numerical simulations with noise. Finally, in sec. V, we conclude our results and discuss possible future directions.

* mori-yuichiro.9302@aist.go.jp

† s-kawabata@aist.go.jp

‡ matsuzaki.yuichiro@aist.go.jp

II. REVIEW OF THE QUANTUM ANNEALING

Let us review the conventional quantum annealing, and consider the following Hamiltonian,

$$\mathcal{H}_{\text{conv}}(t) = f(t)\mathcal{H}_{\text{D}} + (1 - f(t))\mathcal{H}_{\text{P}}, \quad (2)$$

where \mathcal{H}_{D} is a driver Hamiltonian, \mathcal{H}_{P} is a problem Hamiltonian, and $f(t)$ is a schedule function satisfying a condition,

$$f(0) = 1, \quad f(T_{\text{ann}}) = 0, \quad (3)$$

where T_{ann} is called the annealing time. Usually, we choose the function $f(t)$ as

$$f(t) = 1 - \frac{t}{T_{\text{ann}}}. \quad (4)$$

Due to the condition (3), the Hamiltonian at $t = 0$ is the driver Hamiltonian \mathcal{H}_{D} itself and the Hamiltonian at $t = T_{\text{ann}}$ is the problem Hamiltonian itself. After obtaining a ground state of the driver Hamiltonian, we let the state evolve by the annealing Hamiltonian from $t = 0$ to $t = T_{\text{ann}}$. According to the adiabatic theorem, if T_{ann} is large enough, the state after QA becomes a ground state of the problem Hamiltonian.

III. OUR METHOD TO EVALUATE THE ADIABATIC CONDITION

For a quantum system, the dynamics are given by the time-dependent Hamiltonian $\mathcal{H}(t)$. To check whether the dynamics are adiabatic or not, we need to know the denominator and numerator of the Eq. (1). The denominator is an energy gap of the Hamiltonian $\mathcal{H}(t)$, and the numerator is the transition matrix element of $\mathcal{H}(t)$ from the ground state to the m -th excited state of $\mathcal{H}(t)$.

We explain our theoretical proposal to measure these quantities from an experiment. Let us define the following Hamiltonian,

$$\mathcal{H}(t) = \mathcal{H}_{\text{QA}}(t) + \mathcal{H}_{\text{ext}}(t), \quad (5)$$

$$\mathcal{H}_{\text{QA}}(t) = A(t)\mathcal{H}_{\text{D}} + (1 - A(t))\mathcal{H}_{\text{P}} \quad (6)$$

$$\mathcal{H}_{\text{ext}}(t) = \lambda(t)\dot{\mathcal{H}}_{\text{QA}}(t_1) \cos \omega(t - t_1) \quad (7)$$

where \mathcal{H}_{D} is a driver Hamiltonian, \mathcal{H}_{P} is a problem Hamiltonian, $A(t)$ is a schedule function, $\mathcal{H}_{\text{ext}}(t)$ is an external driving Hamiltonian, ω is an angular frequency of the driving field, $\lambda(t)$ is the strength of the driving field, and t_1 is a time to start turning on the external driving. In Fig. 1, we plot $A(t)$ and $\lambda(t)$ against time during our protocol. It is worth mentioning that $A(t)$ coincides with $f(t)$ for $0 < t < t_1$.

Firstly, we prepare a ground state of the driver Hamiltonian $|0(t=0)\rangle$. Secondly, we gradually change the

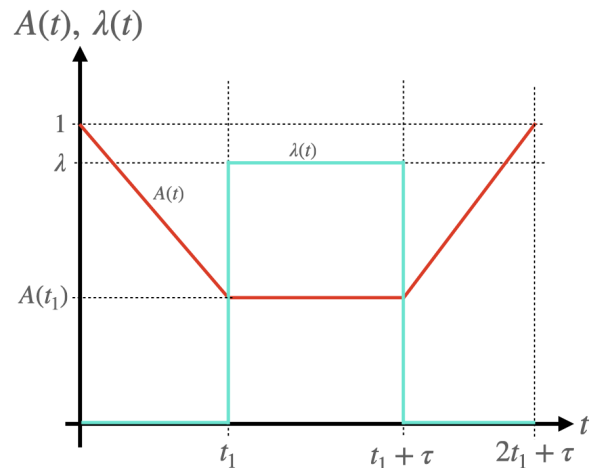


FIG. 1. Plot of the scheduling function $A(t)$ and the strength of the external driving field λ with our protocol.

Hamiltonian $\mathcal{H}_{\text{QA}}(t)$ from $t = 0$ to $t = t_1$ by setting $\lambda(t) = 0$, and the system evolves with the Hamiltonian. Thirdly, at $t = t_1$, we add a driving term to the Hamiltonian by setting $\lambda(t) = \lambda$ while we fix $A(t) = A(t_1)$, and let the system evolve by this Hamiltonian for $t_1 < t < t_1 + \tau$. Fourthly, at $t = t_1 + \tau$, we turn off the driving by setting $\lambda(t) = 0$, and gradually change the Hamiltonian from $\mathcal{H}_{\text{QA}}(t_1)$ to \mathcal{H}_{D} for a time $t_1 + \tau < t < 2t_1 + \tau$, and the system evolves by the Hamiltonian. Fifthly, we perform a projective measurement into the m -th excited state $|m(t=0)\rangle$ of the driver Hamiltonian, and record a measurement result. Finally, repeat these steps many time by changing ω , t_1 , and τ . We define the probability obtained from these procedure as $p_{0,m}(\omega, t_1, \tau)$.

Let us explain how to realize the $\mathcal{H}_{\text{ext}}(t)$ at the third step in the actual experiment. We have

$$\begin{aligned} \mathcal{H}_{\text{ext}}(t) &= \lambda \dot{A}(t_1) \mathcal{H}_{\text{D}} \cos \omega(t - t_1) \\ &\quad - \lambda \dot{A}(t_1) \mathcal{H}_{\text{P}} \cos \omega(t - t_1) \end{aligned} \quad (8)$$

The driver Hamiltonian and problem Hamiltonian can be decomposed by Pauli operators as follows.

$$\mathcal{H}_{\text{D}} = \sum_i h_i \mathcal{O}_i, \quad (9)$$

$$\mathcal{H}_{\text{P}} = \sum_j h'_j \mathcal{O}'_j, \quad (10)$$

where \mathcal{O}_i (\mathcal{O}'_j) denote the Pauli matrices and h_i (h'_j) denotes a time independent coefficient. So we obtain

$$\begin{aligned} \mathcal{H}_{\text{ext}}(t) &= \sum_i \lambda \dot{A}(t_1) h_i \mathcal{O}_i \cos \omega(t - t_1) \\ &\quad - \sum_{j'} \lambda \dot{A}(t_1) h'_j \mathcal{O}'_{j'} \cos \omega(t - t_1) \end{aligned} \quad (11)$$

This means that, if an experimentalist can temporarily change the coefficient of the Pauli matrices as a cosine function, it is possible to realize the Hamiltonian

$\mathcal{H}_{\text{ext}}(t)$. Since the problem Hamiltonian usually contains two-body interaction terms, we need to change the interaction coupling strength. Such a technique has been developed in superconducting circuits [27].

Here, we explain the dynamics of the system in the third step of our scheme, which is crucial to measure the adiabatic condition.

We begin by describing a simplified scenario where the dynamics is adiabatic at the second and fourth step, and we will consider more general cases later. For simplicity, we omit the expression of “(t_1)” to mention $\mathcal{H}_{\text{QA}}(t_1)$ or $\dot{\mathcal{H}}_{\text{QA}}(t_1)$ in the following part of this section. In our proposal, the measurements will be performed by sweeping the time period τ , and so we treat τ as a variable in the remainder of this section unless otherwise mentioned. Let us diagonalize \mathcal{H}_{QA} as follows.

$$\mathcal{H}_{\text{QA}} = \sum_i E_i |i\rangle \langle i|, \quad (12)$$

where $E_i \leq E_j$ is satisfied for $i < j$. By moving to a rotating frame, the state of the system is written as

$$|\tilde{\psi}(\tau)\rangle = e^{is\tau\mathcal{H}_{\text{QA}}} |\psi(\tau)\rangle, \quad (13)$$

and the Hamiltonian in the rotating frame is described as

$$\begin{aligned} \tilde{\mathcal{H}}(\tau) &= e^{is\tau\mathcal{H}_{\text{QA}}} \mathcal{H}(\tau) e^{-is\tau\mathcal{H}_{\text{QA}}} + i \frac{de^{is\tau\mathcal{H}_{\text{QA}}}}{d\tau} e^{-is\tau\mathcal{H}_{\text{QA}}} \\ &= (1-s)\mathcal{H}_{\text{QA}} + e^{is\tau\mathcal{H}_{\text{QA}}} \mathcal{H}_{\text{ext}}(\tau) e^{-is\tau\mathcal{H}_{\text{QA}}}. \end{aligned} \quad (14)$$

It is notable that we set $\hbar = 1$ throughout this paper. Here, we assume that the transition frequency between the ground state and m -th excited state is close to the frequency of the external driving field. Then, we set s as the ratio between $|E_m - E_0|$ and ω as follows.

$$s = \frac{\omega}{|E_m - E_0|} \quad (15)$$

where E_0 denotes the energy of the ground state. The second term in (14) becomes

$$\begin{aligned} &e^{is\tau\mathcal{H}_{\text{QA}}} \mathcal{H}_{\text{ext}}(\tau) e^{-is\tau\mathcal{H}_{\text{QA}}} \\ &= \lambda \sum_{i,j} \langle i|\dot{\mathcal{H}}_{\text{QA}}|j\rangle e^{is(E_i - E_j)\tau} \cos \omega\tau |i\rangle \langle j|. \end{aligned} \quad (16)$$

Here, we are going to apply the rotating wave approximation [28]. The coefficient of $|i\rangle \langle j|$ in the Eq. (16) includes an oscillatory component

$$\begin{aligned} &e^{is(E_i - E_j)\tau} \cos \omega\tau \\ &= \frac{1}{2} e^{is(E_i - E_j)\tau} (e^{i\omega\tau} + e^{-i\omega\tau}) \\ &= \frac{1}{2} e^{i(s(E_i - E_j) - \omega)\tau} + \frac{1}{2} e^{i(s(E_i - E_j) + \omega)\tau}. \end{aligned} \quad (17)$$

We adopt the rotating wave approximation (RWA) to drop high frequency terms. If $s|E_i - E_j| = \omega$ is satisfied,

one of the terms in Eq. (17) becomes time-independent and the other term has a high-frequency oscillation. Due to the condition of (15), we have at least two time-independent terms, $(i, j) = (m, 0)$ and $(0, m)$, to remain after the RWA. We assume a condition $||E_m - E_0| - \omega| \ll ||E_i - E_j| - \omega|$ in neither $(i, j) = (m, 0)$ nor $(i, j) = (0, m)$. Then, by using the RWA, all terms except $(i, j) = (0, m)$ and $(i, j) = (m, 0)$ are dropped. In this case, the Hamiltonian (16) can be simplified to

$$\mathcal{H}_{\text{ext}, I} = \frac{\lambda}{2} \langle m|\dot{\mathcal{H}}_{\text{QA}}|0\rangle |m\rangle \langle 0| + h.c.. \quad (18)$$

Hence, the effective Hamiltonian of Eq. (14) can be written as

$$\mathcal{H}_{\text{eff}} = \sum_i (1-s)E_i |i\rangle \langle i| + \frac{\lambda}{2} \langle m|\dot{\mathcal{H}}_{\text{QA}}|0\rangle |m\rangle \langle 0| + h.c.. \quad (19)$$

From these calculations, it is shown that the dynamics is confined in a subspace spanned by the ground state and the m -th excited state when the initial state is prepared in the subspace. Actually, after performing the first and second step of our method, we can prepare the ground state as the initial state as long as the dynamics is adiabatic. It is worth mentioning that, if we trace out the states except $|E_m\rangle$ and $|E_0\rangle$, the effective Hamiltonian has the same form as the single-qubit Hamiltonian to induce the Rabi oscillation [29]. So we should be able to observe the Rabi oscillation if we implement our protocol. An analytical formula to describe the Rabi oscillation without decoherence is known, and this is characterized by two parameters; detuning and Rabi frequency. (The details of the behavior of Rabi oscillations in a single-qubit system are given in Appendix B.) This means that, by using the analytical formula to describe the Rabi oscillation, we can fit the data obtained from our method, and we can obtain the information of the transition matrix element $|\langle m|\dot{\mathcal{H}}|0\rangle|$ and the energy gap $|E_m - E_0|$.

In order to observe the Rabi oscillation, we need an efficient method to construct a projective measurement of $|m\rangle \langle m|$ in the rotating frame. Actually, in the fourth and fifth step, we effectively construct a projective measurement of $|m\rangle \langle m|$ in the lab frame as long as the dynamics in the fourth step is adiabatic. Moreover, when the state $|\psi(\tau)\rangle$ is an eigenstate of the Hamiltonian \mathcal{H}_{QA} , the change in the frame provides just a global phase. Therefore, as long as the adiabatic condition is satisfied, $p_{0,m}(\omega, t_1, \tau)$ is approximately described as follows

$$\begin{aligned} p_{0,m}(\omega, t_1, \tau) &\simeq |\langle m|e^{-i\tau\mathcal{H}_{\text{eff}}}|0\rangle|^2 \\ &= \alpha(\omega)(1 - \cos \Omega_{\text{ana}}(\omega)\tau), \end{aligned} \quad (20)$$

where $\alpha(\omega)$ is a function of ω given by

$$\alpha(\omega) = \frac{1}{2} \left(\frac{2|\tilde{\lambda}| \left(\Delta - \omega - \sqrt{(\Delta - \omega)^2 + |\tilde{\lambda}|^2} \right)}{\left(\Delta - \omega - \sqrt{(\Delta - \omega)^2 + |\tilde{\lambda}|^2} \right)^2 + |\tilde{\lambda}|^2} \right)^2, \quad (21)$$

$$\Delta = E_m - E_0, \quad \tilde{\lambda} = \lambda \langle m | \dot{\mathcal{H}}_{\text{QA}} | 0 \rangle,$$

and $\Omega_{\text{ana}}(\omega)$ is a hyperbolic curve on the $\omega - \Omega$ plane that is represented by

$$\Omega_{\text{ana}}(\omega) = \sqrt{\left(\lambda |\langle m | \dot{\mathcal{H}}_{\text{QA}} | 0 \rangle|^2 + (\omega - \Delta)^2 \right)}. \quad (22)$$

If the adiabatic condition is satisfied, $p_{0,m}(\omega, t_1, \tau)$ does not have a dependency on t_1 .

In the discussion above, we assume that we prepare a ground state of the driver Hamiltonian at the first step and we perform a projective measurement into the m -th excited states at the fifth step. On the other hand, if we prepare k -th excited state at the first step and perform a projective measurement into the l -th excited states at the fifth step, we can obtain the hyperbolic curve

as $\Omega_{\text{ana}}^{(k,l)}(\omega) = \sqrt{\left(\lambda |\langle l | \dot{\mathcal{H}}_{\text{QA}} | k \rangle|^2 + (\omega - \Delta_{kl})^2 \right)}$ where $\Delta_{kl} = E_k - E_l$ by using similar calculations. The details of these derivations are shown in the Appendix B 1.

The adiabatic condition described in Eq. (1) is valid only when we can treat the effect of the non-adiabatic transitions as a perturbation. So, throughout our paper (except in the Appendix), we assume that the effect of non-adiabatic transitions is negligible. We will discuss how the non-adiabatic transitions affect spectroscopic measurements in our methods later.

Let us explain how to specify the values of $|E_m - E_0|$ and $|\langle m | \dot{\mathcal{H}} | 0 \rangle|$ by using our method. We repeat these by sweeping the ω , and we can find an optimize value of $\omega = |E_m - E_0|$ to minimize the frequency of the Rabi oscillation, and this corresponds to the energy gap Δ . At the same time, the Rabi frequency with the optimal Ω observed in our method corresponds to the numerator Eq. (1). This means that our estimated transition matrix element $|\langle m | \dot{\mathcal{H}} | 0 \rangle|_{\text{est}}$ and our estimated energy gap Δ_{est} should be given by

$$\lambda |\langle m | \dot{\mathcal{H}}_{\text{QA}} | 0 \rangle|_{\text{est}} = \min_{\omega} [\Omega_{\text{exp}}(\omega)], \quad (23)$$

$$\Delta_{\text{est}} = \arg \min_{\omega} [\Omega_{\text{exp}}(\omega)], \quad (24)$$

respectively. Here, $\Omega_{\text{exp}}(\omega)$ is the angular frequency of the Rabi oscillation obtained experimentally, which is analytically considered to be expressed by Eq. (22).

In actual experiments, due to some imperfections, $p_{0,m}(\omega, t_1, \tau)$ cannot be fully explained by the analytical formula Eq. (20), which was derived under ideal conditions (See Fig. 10 in Appendix). To find the relevant frequency of $\Omega_{\text{exp}}(\omega)$ in the dynamics, we perform a Fourier

transformation, and we obtain a power spectrum, which is defined by

$$P(\omega, t_1, \Omega) = \text{abs} [\text{FT}[p_{0,m}(\omega, t_1, \tau)]], \\ = \text{abs} \left[\int_{-\infty}^{\infty} d\tau p_{0,m}(\omega, t_1, \tau) \frac{e^{-i\Omega\tau}}{\sqrt{2\pi}} \right]. \quad (25)$$

If $p_{0,m}(\omega, t_1, \tau)$ is expressed as the Eq. (20), the power spectrum is given as

$$P(\omega, t_1, \Omega) = \alpha(\omega) \delta(\Omega) + \frac{\alpha(\omega)}{2} \delta(\Omega - \Omega_{\text{ana}}(\omega)) \\ + \frac{\alpha(\omega)}{2} \delta(\Omega + \Omega_{\text{ana}}(\omega)). \quad (26)$$

So, in the actual experiment, we define the peak with a positive frequency in the spectrum as $\Omega_{\text{exp}}(\omega)$, and we expect to satisfy $\Omega_{\text{exp}}(\omega) \simeq \Omega_{\text{ana}}(\omega)$ in the power spectrum, and this allows us to use the formulas of Eqs. (23) and (24). This is how we could estimate the values of the transition matrix element $|\langle m | \dot{\mathcal{H}}_{\text{QA}} | 0 \rangle|$ and the energy gap Δ with our method.

IV. NUMERICAL ANALYSIS

To quantify the performance of our method, we implement numerical simulations of the proposed method described in the previous section. To obtain an analytical formula in the previous section, we assumed the following conditions.

- I. The dynamics in steps 2 and 4 are adiabatic
- II. The rotating wave approximation is valid
- III. The dynamics in step 3 occurs in a two-level subspace
- IV. There is no decoherence.

However, in actual experiments, these conditions are not always satisfied. So we will perform numerical simulations when some (or all) of these conditions are not met. We summarize the conditions for numerical simulations to be performed I.

Case	Qbit Number	Adiabaticity of Step 2 and 4	Decoherence	Violated conditions
A	1	Complete	None	II
B	1	Imcomplete	None	I, II
C	1	Imcomplete	✓	I, II, IV
D	2	Complete	None	II, III
E	2	Imcomplete	None	I, II, III
F	2	Imcomplete	✓	I, II, III, IV

TABLE I. List of cases studied in this work. For the case B, C, E, and F, we consider the effect of non-adiabatic transitions at the step 2 and 4. On the other hand, for the case of C and F, we take into account decoherence.

The condition I is satisfied when the process at the step 2 and 4 is completely adiabatic. Although we can solve a time dependent Schrodinger equation with a long annealing time, instead, we diagonalize the Hamiltonian to prepare a ground state as the initial state at the step 3. Especially, for cases A and D in Table I, we prepare the ground state of $\mathcal{H}_{\text{QA}}(t_1)$ by the diagonalization at the step 3.

The condition III can be naturally satisfied for a single qubit system. On the other hand, this condition is violated for a system with two or more qubits. Thus, in cases A, B, and C using a single qubit system, the condition III is satisfied, but in cases D, E, and F, condition III is violated.

The condition IV is satisfied if we solve a time-dependent Schrodinger equation of the system, which are the cases of A, B, D and E. On the other hand, we consider the effect of decoherence by solving the master equation in the cases C and F.

A. Settings and methods for all cases

Here, we introduce some conditions common to all of our numerical analysis.

1. Schedule function

For the schedule function $A(t)$ in Eq. (5), we use

$$A(t) = \begin{cases} 1 - \frac{t}{T_{\text{ann}}} & (0 \leq t < t_1) \\ 1 - \frac{t_1}{T_{\text{ann}}} & (t_1 \leq t < t_1 + \tau), \\ \frac{t - \tau - 2t_1}{T_{\text{ann}}} + 1 & (t_1 + \tau \leq t < 2t_1 + \tau) \end{cases} \quad (27)$$

where T_{ann} is the annealing time. In the actual experiments, this value is typically around 10 to 100 μs , and a typical energy scale of the Hamiltonian is an order of GHz [30].

We take the schedule function (27) as $A(t) = 1 - t/T_{\text{ann}}$ up to T_{ann} and we evaluate the adiabatic condition at time t_1 according to our method. Hence, for our simulation, $\dot{\mathcal{H}}_{\text{QA}}(t_1)$ is given by

$$\dot{\mathcal{H}}_{\text{QA}}(t_1) = -\frac{1}{T_{\text{ann}}}\mathcal{H}_{\text{D}} + \frac{1}{T_{\text{ann}}}\mathcal{H}_{\text{P}}, \quad (28)$$

for any t_1 .

2. Strength λ

Since we have

$$\lambda |\langle m | \dot{\mathcal{H}}_{\text{QA}} | 0 \rangle| \propto \frac{\lambda}{T_{\text{ann}}}, \quad (29)$$

the Rabi frequency can be controlled by changing the value of $\frac{\lambda}{T_{\text{ann}}}$ where we substitute Eq. (28). If decoherence is negligible, we should set $\frac{\lambda}{T_{\text{ann}}}$ as small as possible, because the RWA is valid only when the Rabi frequency is much smaller than the energy gap Δ . On the other hand, when there is decoherence, the choice of λ/T_{ann} is not so straightforward. As we decrease λ/T_{ann} , the decoherence becomes more relevant while the RWA becomes more valid. So we need to satisfy the following condition.

$$\frac{1}{T_c T_{\text{ann}} |\langle m | \dot{\mathcal{H}}_{\text{QA}} | 0 \rangle|} \ll \frac{\lambda}{T_{\text{ann}}} \ll 1, \quad (30)$$

where T_c is the coherence time. In our simulation, we used

$$\frac{\lambda}{T_{\text{ann}}} = 0.05. \quad (31)$$

3. Time evolution and Measurement process

In the actual experiments, we should take decoherence into account. For this purpose, we adopt the Gorini-Kossakowski-Sudarshan-Lindblad (GKSL) master equation [31],

$$\dot{\rho} = -i[\mathcal{H}, \rho] + \sum_n (L_n \rho L_n^\dagger - \frac{1}{2}\{L_n^\dagger L_n, \rho\}), \quad (32)$$

for the cases C and F, where L_n are the Lindblad operators.

At the fifth step we perform a projective measurement into the state $|m(t=0)\rangle$. Unless otherwise mentioned, we set $m = 1$, because the non-adiabatic transition from the ground state to the first excited state is usually the main concern for QA.

4. Construction of $\Omega_{\text{exp}}(\omega)$

In our method, we calculate a projection probability into the first excited state $p_{0,1}(\tau)$ and we make the power spectrum $P(\Omega)$ to determine the function $\Omega_{\text{exp}}(\omega)$ as we explained in the previous section. In this case, we expect to observe a peak at $\Omega = \Omega_{\text{ana}}(\omega)$ in the power spectrum. To determine the function $\Omega_{\text{exp}}(\omega)$, we fix ω and maximize height of the power spectrum by sweeping Ω so that we can determine the position of the resonance peak as

$$\Omega_{\text{exp}}(\omega) = \arg \max_{\Omega} P(\Omega, \omega). \quad (33)$$

Finally, by sweeping ω , we can obtain the function $\Omega_{\text{exp}}(\omega)$.

When we sweep Ω , we should consider an appropriate range as follows. First, we sweep the frequency range of $\Omega > 0$. As we have already seen in Eq. (26), there are three peaks. However, to evaluate the adiabatic condition, we can focus only the peak at positive frequency,

because the peak at negative frequency has the same information as that at positive frequency while the peak at zero frequency does not contain information. Second, we sweep the frequency range of $\Omega \ll \omega$. We use the RWA to derive the analytical formula of (20), but this is valid only for $\Omega \ll \omega$.

Even if we restrict the frequency range, we may fail to find a correct peak for several reasons. We will discuss the case when such a problem occurs, and show a possible solution to overcome such a problem at least for some cases.

B. Single-qubit cases (Case A, B, C)

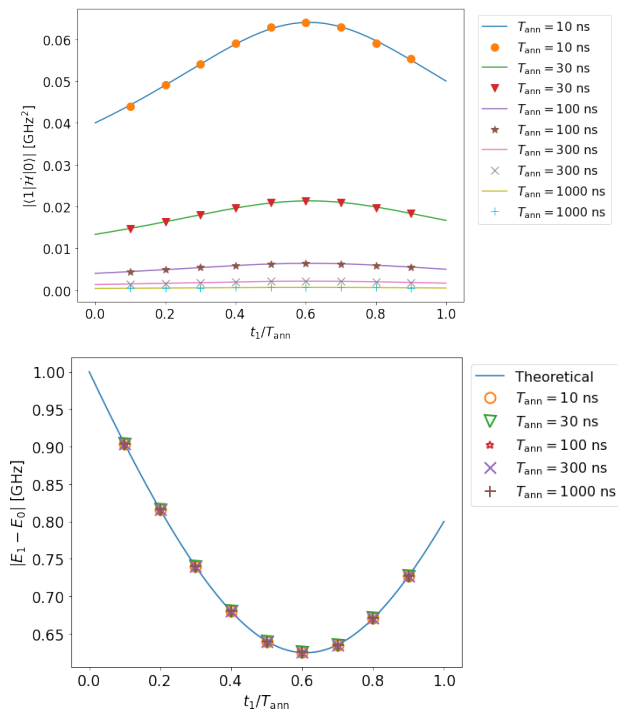


FIG. 2. (Top) An estimation of the transition matrix element in case A (single qubit, complete adiabaticity, and no decoherence). The solid lines are the solution obtained by diagonalization of the Hamiltonian, and the dots are the estimated values obtained from our method by numerical simulations. (Bottom) An estimation of the energy gap in case A. The solid line is the solution obtained by diagonalization of the Hamiltonian, and the dots are the estimated values obtained from our scheme by numerical simulations.

We see the single-qubit cases (Case A, B, C). For these cases, the driver Hamiltonian \mathcal{H}_D and the problem Hamiltonian \mathcal{H}_P are given as

$$\mathcal{H}_D = \frac{\omega_1}{2} \sigma_x, \quad \mathcal{H}_P = g \sigma_z, \quad (34)$$

respectively. In our simulation, we fixed $\omega_1 = 1$ GHz and $g = 0.4$ GHz.

1. Case A

We set the parameters T_{ann} and t_1/T_{ann} as

$$\begin{aligned} T_{\text{ann}} &= 10, 30, 100, 300, 1000 \text{ ns}, \\ t_1/T_{\text{ann}} &= 0.1, 0.2, 0.3, 0.4, \dots, 0.9. \end{aligned} \quad (35)$$

As we can see in Fig. 2, our estimated values (dots in the figure) are in good agreement with the theoretically expected values (lines in the figure). Indeed, the relative error in the estimation of the transition matrix element $|\langle 1|\mathcal{H}|0\rangle|$ (the energy gap $E_1 - E_0$) is at most 0.99% (0.071%).

These errors are small compared to the resolution due to the discretization performed in processing the data. The estimation error of the transition matrix element (energy gap) is 0.9 (0.1) times smaller than the resolution. Actually in Fig. 2, we confirm that the adiabatic condition (1) is reasonably satisfied.

2. Case B

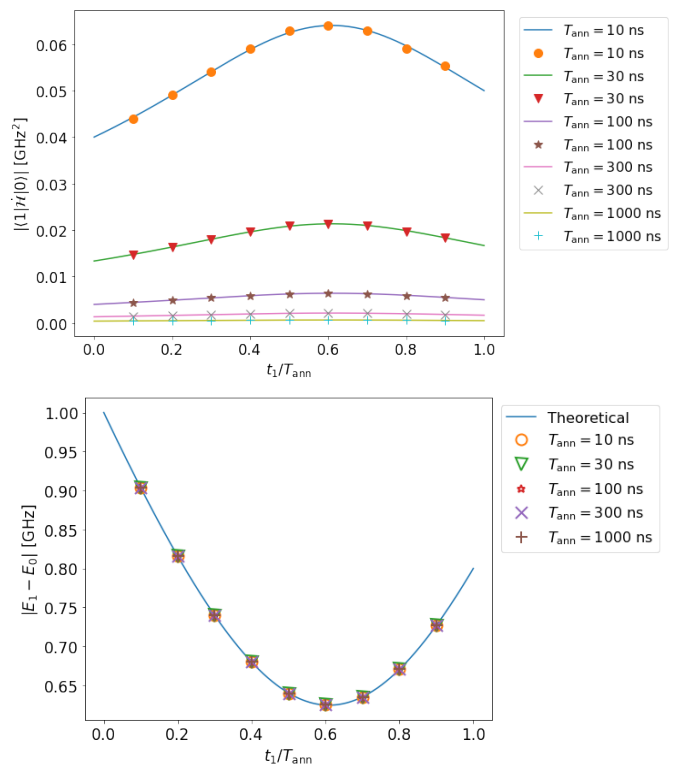


FIG. 3. At the top (bottom), we plot the estimated value of the transition matrix element (energy gap) in case B (single qubit, incomplete adiabaticity, and no decoherence).

Next, the effect of non-adiabatic transitions in steps 2 and 4 is studied for the case B. Similar to the case A, we can accurately measure both the transition matrix element $|\langle 1|\mathcal{H}|0\rangle|$ and the energy gap $(E_1 - E_0)$ for the

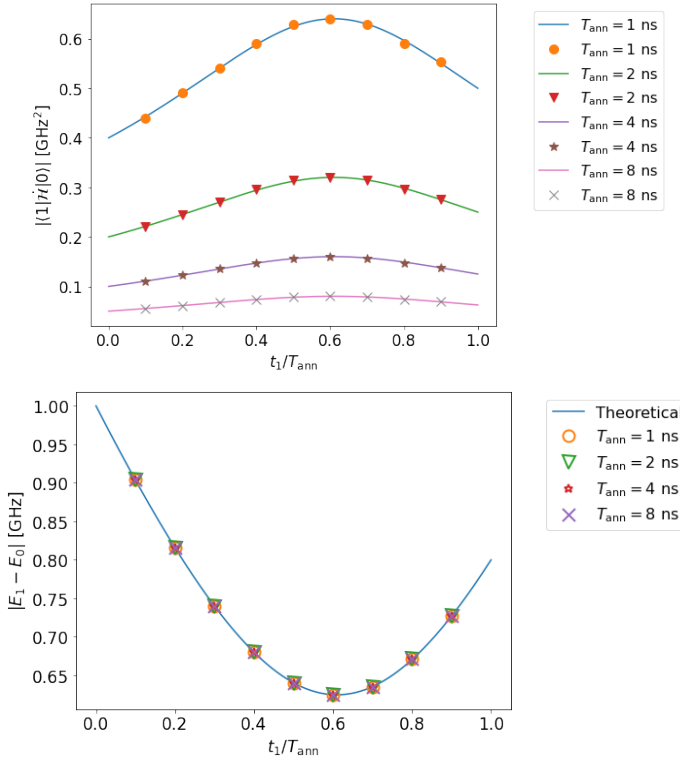


FIG. 4. At the top (bottom), we plot the estimated value of the transition matrix element (energy gap) in case B (single qubit, incomplete adiabaticity, and no decoherence) with a shorter annealing time such as $T_{\text{ann}} = 1, 2, 4, 8$ ns.

case B, and (See Fig. 3) the relative error of the transition matrix element (energy gap) is a maximum of 2.2% (0.7%) and 0.77 (0.93) relative to the resolution.

For the single qubit case, our scheme is robust against the non-adiabatic transitions. Actually, we consider cases with $T_{\text{ann}} = 1, 2, 4,$ and 8 ns (see Fig. 4), and these results show that the shorter annealing time dose not impair the performance of our methods.

Actually, we show that, as long as the RWA is valid, the power spectrum contains a peak corresponding to a frequency of $\Omega(\omega)$ (See Appendix B 2). This means that we can accurately estimate the transition matrix element and energy gap by using Eqs. (23) and (24) for the single-qubit case without decoherence.

3. Case C

In the case C, to take into account decoherence, we adopt the GKSL master equation, and we choose the Lindblad operator as

$$L = \sqrt{\kappa}\sigma_z, \quad (36)$$

where κ denotes the decay rate. We fix $\kappa = 2.5 \times 10^{-3}$ ns $^{-1}$ which is a typical value for a superconducting flux qubit [32].

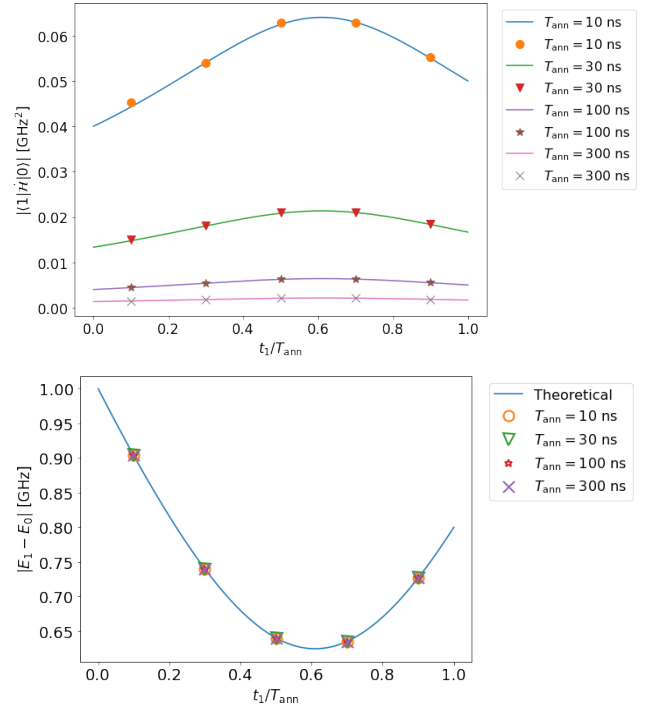


FIG. 5. At the top (bottom), we plot the estimated value of the transition matrix element (energy gap) in case C (single qubit, incomplete adiabaticity, and with decoherence)

We represent the results in Fig. 5. The relative error of the transition matrix element $|\langle 1|\hat{H}|0\rangle|$ (the energy gap Δ) is at most 2.1% (0.05%). This is 0.77 (0.023) times smaller than the resolution.

These errors are as small as those in cases A and B, and so our method is robust against decoherence. This is due to the fact that decoherence does not affect the position but the width of the peaks in the power spectrum. So an accurate estimation of the transition matrix element and energy gap is possible even under the effect of decoherence as long as decoherence is weak.

C. Two-qubit cases (D, E, F)

In the two-qubit cases, the problem and driver Hamiltonians are given as

$$\begin{aligned} \mathcal{H}_D &= \frac{\omega_1}{2}\sigma_x \otimes 1 + \frac{\omega_2}{2}1 \otimes \sigma_x, \\ \mathcal{H}_P &= g_1\sigma_z \otimes \sigma_z + g_2\sigma_z \otimes 1 + g_31 \otimes \sigma_z. \end{aligned} \quad (37)$$

respectively. Here, we set $\omega_1 = 1.0$ GHz, $\omega_2 = 1.1$ GHz, $g_1 = 0.5$ GHz, $g_2 = 0.3$ GHz, and $g_3 = 0$.

For these cases, we choose the parameters T_{ann} and t_1 as follows.

$$\begin{aligned} T_{\text{ann}} &= 10, 30, 100 \text{ ns}, \\ t_1/T_{\text{ann}} &= 0.1, 0.3, 0.5, 0.7, 0.9. \end{aligned} \quad (38)$$

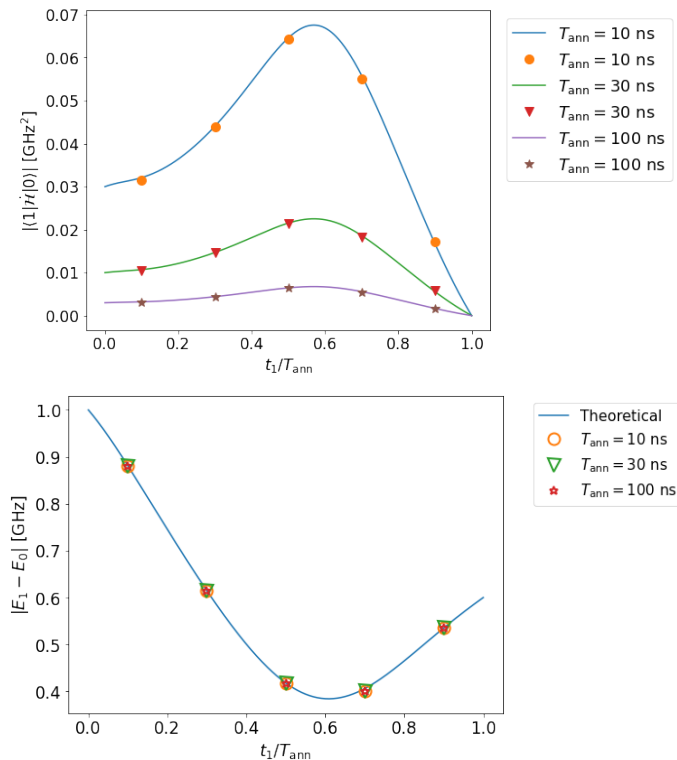


FIG. 6. At the top (bottom), we plot the estimated value of the transition matrix element (energy gap) in case D (two qubit, complete adiabaticity, and no decoherence). Even when two-qubit is used, we can estimate well both the transition matrix element and the energy gap with high accuracy.

1. Case D

In this case, we can accurately measure the transition matrix element $|\langle 1|\hat{\mathcal{H}}|0\rangle|$ and energy gap ($E_1 - E_0$) as shown in Fig. 6. The relative error of the transition matrix element (energy gap) is at most 3.5% (0.04%). This is 0.55 (0.99) times smaller than the resolution. Although the condition III is not satisfied in this case to consider the two qubits, the dynamics can be approximately confined in a two-level system as long as the Rabi frequency is small. This explains the accuracy of our method.

2. Case E

In the case E, the relative error of the transition matrix element (energy gap) is at most 3.5% (1.2%). This is 0.55 (0.99) times smaller than the resolution as shown in 7.

In the case of weak nonadiabatic transitions, it is possible to estimate both the transition matrix elements and energy gap with high accuracy even for the two-qubit case. On the other hand, as described in detail in Appendix C, in the case of strong nonadiabatic transitions, the power spectrum contains peaks other than the one we want to use in our estimation. We discuss possible

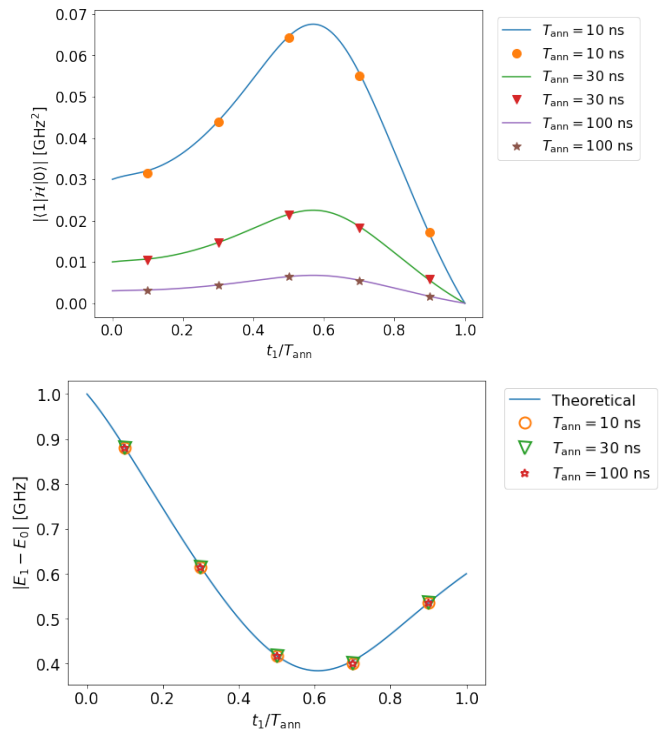


FIG. 7. At the top (bottom), we plot the estimated value of the transition matrix element (energy gap) in case E (two qubit, incomplete adiabaticity, and no decoherence).

solution for this in Appendix C.

3. Case F

In the case F, we choose the Lindblad operators as follows.

$$L_1 = \sqrt{\kappa}\sigma_z \otimes 1, \quad L_2 = \sqrt{\kappa}1 \otimes \sigma_z, \quad (39)$$

where κ denotes the decay rate. For the numerical simulations, we choose $\kappa = 2.5 \times 10^{-3} \text{ ns}^{-1}$.

We plot the estimated transition matrix element and energy gap against t_1/T_{ann} , and show that our method is accurate except for two points, $t_1/T_{\text{ann}} = 0.3$ and $t_1/T_{\text{ann}} = 0.9$ for $T_{\text{ann}} = 100 \text{ ns}$, as shown in Fig. 8.

In the former case, as shown in the power spectrum (see Fig. 9 (a)), where ω is smaller than 0.575 or larger than 0.65, a low frequency ($\Omega < 0.02$) peak exist and the height of this peak is higher than the target peak at the same ω . As shown in Eq. (26), strictly speaking, a peak around $\Omega \simeq 0$ should exist in the spectrum, and this peak has a finite width due to decoherence so that we can observe this in case F. So, if we naively adopt our method described in Eq. (33), we generate an inappropriate $\Omega_{\text{exp}}(\omega)$ and obtain wrong estimated values about the transition matrix element and energy gap.

To identify the target peak under the effect of decoherence and non-adiabatic conditions, we adopt the modified

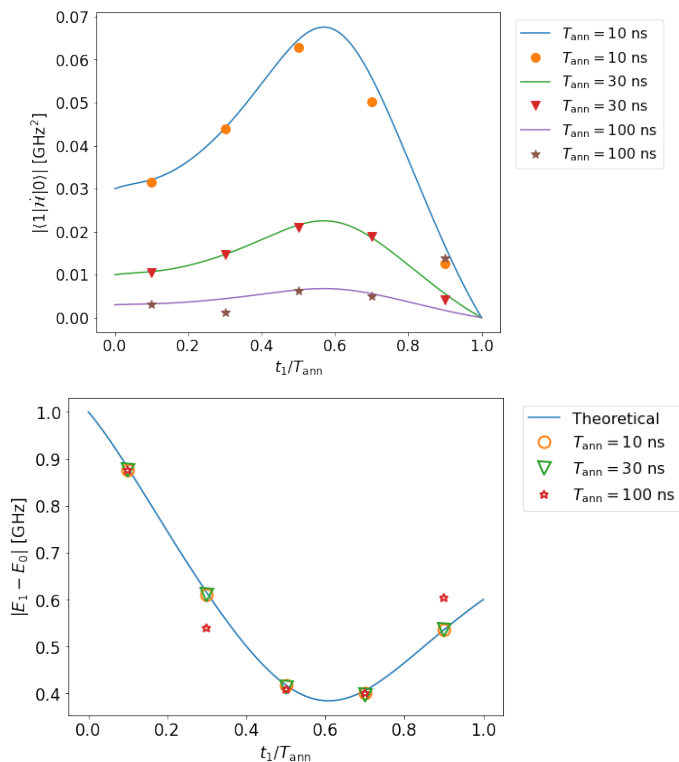


FIG. 8. At the top (bottom), we plot the estimated value of the transition matrix element (energy gap) in case F (two qubit, incomplete adiabaticity, and with decoherence). In this case, we have significant estimation errors for a few points.

method as follows. First, we evaluate the value of Ω of not only the highest peak but also the second and the third highest peaks for each ω and these values (ω, Ω) become candidates of the data of the estimated function $\Omega_{\text{exp}}(\omega)$. Second, we try to fit the data with the analytical formula of Eq. (22). Third, we remove data that we cannot fit by the analytical formula. Finally, we choose data that are fit by the analytical formula, and consider this as the target peaks.

In the former case, after using this modified method, the relative error of the transition matrix element (energy gap) is 1.0% (0.2%) and the ratio to the resolution is 0.07 (0.26). This shows that our modified method is effective for this case.

In the latter case, however, decoherence is so strong that the target peak almost disappears, and we cannot identify the target peak anymore, as shown in Fig. 9 (b).

V. CONCLUSION AND DISCUSSION

In conclusion, we propose an experimental method to check whether an adiabatic condition is satisfied. Our method uses an oscillating field to induce Rabi oscillations in the middle of quantum annealing. This process provides information on the energy gap and the transition

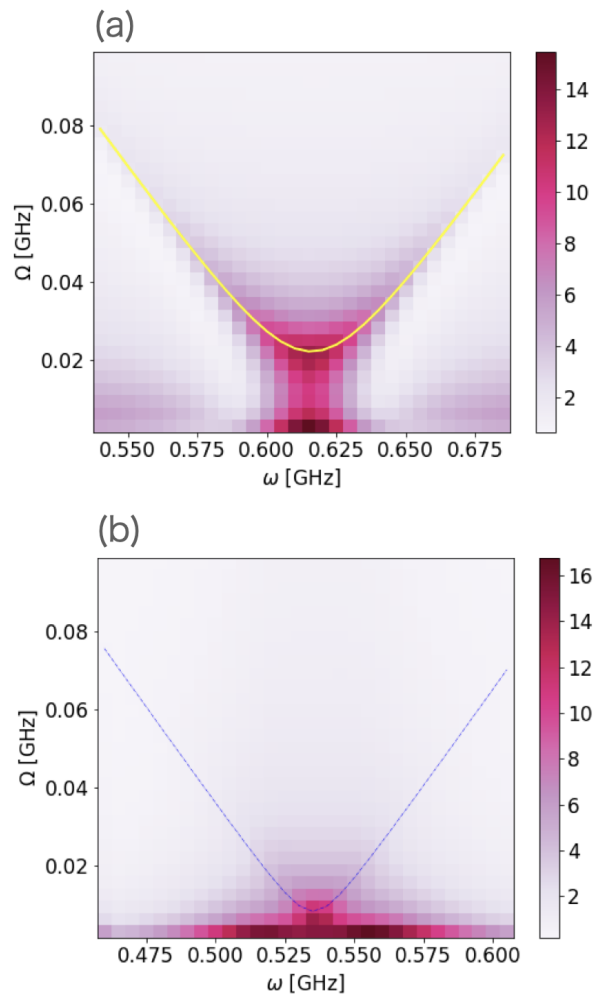


FIG. 9. Plot of the power spectrum $P(\omega, \Omega)$ for $T_{\text{ann}} = 100$ for case F (two qubit, incomplete adiabaticity, and with decoherence). The horizontal axis denotes the angular frequency, and the vertical axis denotes the Fourier frequency. (a) We use $t_1/T_{\text{ann}} = 0.3$. The yellow line is obtained by fitting equation (22) to the plot. (b) We use $t_1/T_{\text{ann}} = 0.9$. The dotted line depicts the exact value obtained by diagonalization.

matrix element of the time derivative of the Hamiltonian. Also, we quantify the performance of our method by implementing numerical simulations. We mainly investigate how non-adiabatic transitions and decoherence affect the estimation of the adiabatic condition. Our results show the robustness of our method against such imperfections.

Our method is useful for finding suitable annealing scheduling and form of the Hamiltonian to improve the performance of quantum annealing. When the phase transition occurs, the performance of quantum annealing worsens. There are some proposals to avoid it during quantum annealing for specific cases [33–35]. To adopt these methods, we need to change the annealing scheduling and form of the Hamiltonian. However, the potential problem is that we cannot easily optimize the annealing

scheduling and form of the Hamiltonian for general problems if we do not know whether the adiabatic condition is satisfied. On the other hand, by using our methods to evaluate the adiabaticity of the dynamics, we may choose suitable annealing scheduling and form of the Hamiltonian when we try to solve practical optimization problems using quantum annealing. We leave the detailed analysis for future work.

ACKNOWLEDGMENTS

We are grateful to Takashi Imoto, Hideaki Okane, Hiroshi Hayasaka, and Tadashi Kadowaki for insightful discussions.

This work was supported by Leading Initiative for Excellent Young Researchers MEXT Japan and JST presto (Grant No. JPMJPR1919) Japan. This paper is partly based on results obtained from a project, JPNP16007, commissioned by the New Energy and Industrial Technology Development Organization (NEDO), Japan.

We thank the developers of QuTiP [36], which was used for numerical simulations.

Appendix A: Adiabatic theorem and adiabatic condition

In this section, we review the adiabatic theorem. We consider a time-dependent Hamiltonian $\mathcal{H}(t)$. For each time t , we denote the eigenstates (called instantaneous eigenstates) obtained by diagonalizing the Hamiltonian $\mathcal{H}(t)$ as $|n(t)\rangle$ and eigenvalues (called instantaneous energy) as $E_n(t)$.

$$\mathcal{H}(t) |n(t)\rangle = E_n(t) |n(t)\rangle \quad (\text{A1})$$

For any state $|\psi(t)\rangle$, at each time t , the state can be expanded using the instantaneous eigenstates $|n(t)\rangle$ as

$$|\psi(t)\rangle = \sum_n c_n(t) e^{-it\bar{E}_n(t)} |n(t)\rangle, \quad (\text{A2})$$

where $\bar{E}_n(t)$ is defined by

$$\bar{E}_n(t) = \frac{1}{t} \int_0^t d\tau E_n(\tau). \quad (\text{A3})$$

If this $|\psi(t)\rangle$ is a solution that satisfies the Schrodinger equation, we obtain

$$\begin{aligned} i \frac{d}{dt} |\psi(t)\rangle &= i \sum_n \frac{d}{dt} (c_n(t) e^{-it\bar{E}_n(t)} |n(t)\rangle) \\ &= i \sum_n \dot{c}_n(t) e^{-it\bar{E}_n(t)} |n(t)\rangle \\ &\quad + (-i \frac{d}{dt} (t\bar{E}_n(t))) c_n(t) e^{-it\bar{E}_n(t)} |n(t)\rangle \\ &\quad + c_n(t) e^{-it\bar{E}_n(t)} |\dot{n}(t)\rangle \\ &= \sum_n c_n(t) E_n(t) e^{-it\bar{E}_n(t)} |n(t)\rangle. \end{aligned} \quad (\text{A4})$$

Combining (A4) and the orthonormality of the eigenstates, we obtain

$$i \dot{c}_n(t) e^{-it\bar{E}_n(t)} + i \sum_m c_m(t) e^{-it\bar{E}_m(t)} \langle n(t) | \dot{m}(t) \rangle = 0. \quad (\text{A5})$$

Now differentiate both sides of (A1) at time t .

$$\dot{\mathcal{H}}(t) |n(t)\rangle + \mathcal{H}(t) |\dot{n}(t)\rangle = \dot{E}_n(t) |n(t)\rangle + E_n(t) |\dot{n}(t)\rangle \quad (\text{A6})$$

By taking the inner product with $|m(t)\rangle$ again, (A5) becomes

$$\begin{aligned} \dot{c}_n(t) + \langle n(t) | \dot{n}(t) \rangle c_n(t) \\ = \sum_{m \neq n} \frac{\langle n(t) | \dot{\mathcal{H}} | m(t) \rangle}{E_n(t) - E_m(t)} c_m(t) e^{it(\bar{E}_n(t) - \bar{E}_m(t))}. \end{aligned} \quad (\text{A7})$$

When we neglect the right-hand side of (A7), we can get the adiabatic theorem. Indeed, it is clear that no transitions between the energy levels occur in this time evolution, because differential the equation contains only one variable $c_n(t)$.

To obtain the final state after the time evolution, we integrate both sides of Eq. (A7) and we obtain

$$\begin{aligned} c_n(t) - c_n(0) &= - \int_0^t \langle n(\tau) | \dot{n}(\tau) \rangle c_n(\tau) d\tau \\ &\quad + \int_0^t \sum_{m \neq n} \frac{\langle n(\tau) | \dot{\mathcal{H}} | m(\tau) \rangle}{E_n(\tau) - E_m(\tau)} c_m(\tau) e^{i\tau(\bar{E}_n(\tau) - \bar{E}_m(\tau))} d\tau. \end{aligned} \quad (\text{A8})$$

If necessary, we perform a transformation of the basis $|\tilde{n}(t)\rangle = e^{i\theta(t)} |n(t)\rangle$, and $\langle n(t) | \dot{n}(t) \rangle$ can be zero. By using this, Eq. (A8) becomes

$$\begin{aligned} c_n(t) - c_n(0) \\ = \int_0^t \sum_{m \neq n} \frac{\langle n(\tau) | \dot{\mathcal{H}} | m(\tau) \rangle}{E_n(\tau) - E_m(\tau)} c_m(\tau) e^{i\tau(\bar{E}_n(\tau) - \bar{E}_m(\tau))} d\tau. \end{aligned} \quad (\text{A9})$$

By recursive use of (A9), we obtain a form of $c_n(t)$ as an infinite series. If we use the first order perturbation, we obtain

$$\begin{aligned} c_n(t) \\ \simeq c_n(0) + \sum_{m \neq n} c_m(0) \int_0^t \frac{\langle n(\tau) | \dot{\mathcal{H}} | m(\tau) \rangle}{E_n(\tau) - E_m(\tau)} e^{i\tau(\bar{E}_n(\tau) - \bar{E}_m(\tau))} d\tau \\ = c_n(0) - i \sum_{m \neq n} c_m(0) (A_{mn}(t) - A_{mn}(0) + B_{mn}(t)), \end{aligned} \quad (\text{A10})$$

where

$$A_{mn}(t) = \frac{\langle n(t)|\dot{\mathcal{H}}|m(t)\rangle}{(E_n(t) - E_m(t))^2} e^{it(\bar{E}_n(t) - \bar{E}_m(t))}, \quad (\text{A11})$$

$$B_{mn}(t) = \int_0^t \frac{e^{i\tau(\bar{E}_n(\tau) - \bar{E}_m(\tau))}}{E_n(\tau) - E_m(\tau)} \frac{d}{d\tau} \left[\frac{\langle n(\tau)|\dot{\mathcal{H}}|m(\tau)\rangle}{E_n(\tau) - E_m(\tau)} \right] d\tau. \quad (\text{A12})$$

Here, we use

$$\frac{d}{dt} [t(\bar{E}_n(t) - \bar{E}_m(t))] = E_n(t) - E_m(t). \quad (\text{A13})$$

When (1) is satisfied, $A_{mn}(t)$ is negligible. Of course, in general, if $B_{mn}(t)$ is nonzero, $c_n(t)$ is different from $c_n(0)$ in the first order perturbation so that the adiabaticity is not always guaranteed by Eq. (1) [3]. However, if E_n and E_m are time independent, $B_{mn}(t)$ corresponds to a Fourier transformation, and so $B_{mn}(t)$ can be negligible unless the integrating function includes a component whose angular frequency is corresponding to the (average) energy gap $\bar{E}_n - \bar{E}_m$. Except for the special non-negligible B_{mn} case, the condition (1) makes $c_n(t) = c_n(0)$ and it shows the statement of the adiabatic theorem.

Usually, when we consider the quantum annealing, the initial states are designated by

$$c_0 = 1, \quad c_n = 0 \quad (n \neq 0), \quad (\text{A14})$$

so that we can finally obtain

$$c_0(t) = 1, \quad c_n(t) = -i(A_{0n}(t) - A_{0n}(0)). \quad (\text{A15})$$

and $c_n(t) \simeq 0$ if the change in the Hamiltonian is slow enough.

Appendix B: Rabi oscillation

We focused on the characteristics of the dynamics of the system in our proposal. As we explained in the main text, our scheme for a single qubit is equivalent to the conventional Rabi oscillation as long as the dynamics are adiabatic. On the other hand, if non-adiabatic transitions occur, the observed dynamics in our scheme deviate from the Rabi oscillation. We will explain these points.

1. Conventional Rabi oscillation

Based on the discussion in the main text, we consider a Rabi oscillation between the state $|k\rangle$ and $|l\rangle$. (For example, the Hamiltonian in Eq. (19) corresponds to a case with $k = 0$ and $l = m$.) We have

$$\mathcal{H}_{\text{eff}} = (1-s)\frac{\Delta}{2}\sigma_z + \frac{\tilde{\lambda}}{2}|k\rangle\langle l| + \frac{\tilde{\lambda}^*}{2}|l\rangle\langle k|, \quad (\text{B1})$$

where $\sigma_z = |l\rangle\langle l| - |k\rangle\langle k|$, $\Delta = E_l - E_k$ and $\tilde{\lambda} = \lambda\langle l|\dot{\mathcal{H}}_{\text{QA}}|k\rangle$. This coincides with the conventional Hamiltonian to induce the Rabi oscillation where $\tilde{\lambda}$ denotes the Rabi frequency and $(1-s)\Delta$ denotes the detuning. For this Hamiltonian, the operation $e^{i\theta\sigma_z}$ is applied to rotate it around the z -axis by an appropriate angle θ . Then, the Hamiltonian (B1) can become

$$\mathcal{H}_{\text{eff}} = (1-s)\frac{\Delta}{2}\sigma_z + \frac{|\tilde{\lambda}|}{2}\sigma_x, \quad (\text{B2})$$

where $\sigma_x = |k\rangle\langle l| + |l\rangle\langle k|$. We can rewrite (B2) with a unitary operator U_{diag} as

$$\mathcal{H}_{\text{eff}} = \frac{\tilde{\lambda}'}{2}U_{\text{diag}}^\dagger\sigma_x U_{\text{diag}}, \quad (\text{B3})$$

where $\tilde{\lambda}'$ satisfies with an equation

$$\frac{\tilde{\lambda}'}{2} = \sqrt{\left(\frac{|\tilde{\lambda}|}{2}\right)^2 + \left((1-s)\frac{\Delta}{2}\right)^2}, \quad (\text{B4})$$

By setting $s = \omega/\Delta$, we obtain $\tilde{\lambda}' = \Omega_{\text{ana}}^{(k,l)}(\omega)$ in the Eq. (22).

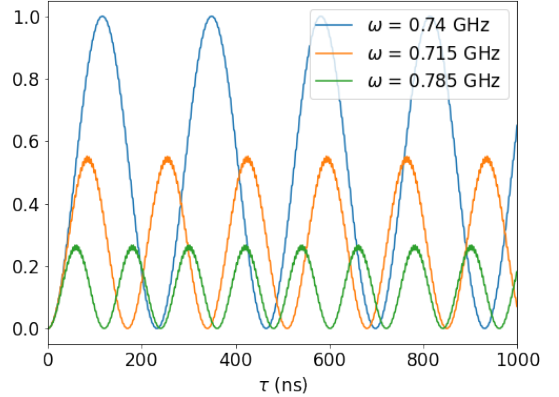


FIG. 10. Plot of the Rabi oscillation. We use a single-qubit Hamiltonian (34), $T_{\text{ann}} = 30$ and $t_1 = 0.3T_{\text{ann}}$. The oscillation period becomes the longest when the angular frequency ω of the external field coincides with the energy gap $\Delta = 0.74$, indicating that the oscillation period is shorter for small angular frequencies ($\omega = 0.715$) and also for large angular frequencies ($\omega = 0.785$).

To observe Rabi oscillations, we calculate the amplitude,

$$\begin{aligned} \langle l|e^{-it\mathcal{H}_{\text{eff}}}|k\rangle &= \langle l|U_{\text{diag}}^\dagger e^{-it\frac{\tilde{\lambda}'}{2}\sigma_x} U_{\text{diag}}|k\rangle, \\ &= -i\sin\frac{\tilde{\lambda}'}{2}t \langle l|U_{\text{diag}}^\dagger\sigma_x U_{\text{diag}}|k\rangle, \end{aligned} \quad (\text{B5})$$

with using relations,

$$e^{i\theta\sigma_x} = \cos\theta + i\sin\theta\sigma_x, \quad (\text{B6})$$

$$\langle l|U_{\text{diag}}^\dagger U_{\text{diag}}|k\rangle = 0. \quad (\text{B7})$$

Finally, we obtain,

$$|\langle l|e^{-it\mathcal{H}_{\text{eff}}}|k\rangle|^2 = |\langle l|U_{\text{diag}}^\dagger\sigma_x U_{\text{diag}}|k\rangle|^2 \frac{1 - \cos\tilde{\lambda}'t}{2}. \quad (\text{B8})$$

Due to the form of Eq. (B4), the minimum value of $\tilde{\lambda}'$ is given by $s = 1$ and then, the angular frequency of the Rabi oscillation $\tilde{\lambda}'$ is $|\tilde{\lambda}'| = \lambda|\langle l|\mathcal{H}|k\rangle|$. In this case, $U_{\text{diag}} = I$ and the amplitude is maximized. This indicates that the Rabi oscillation is a kind of resonance phenomenon whose resonant angular frequency is the energy gap Δ .

When the dynamics at the second and fourth step is adiabatic, both the initial state and the final state are energy eigenstates and it is the case. On the other hand, Fig. 10 shows that the Rabi oscillations were obtained numerically using the Hamiltonian induced by (34) directly, without using the approximation described in this section. It is generally a simple sinusoidal curve, but there are slight fine oscillations when looking at the details.

2. Dynamics with non-adiabatic conditions

We explain the dynamics of our system when the non-adiabatic transitions occur at the second and fourth step. Here, for simplicity, we assume that the RWA is valid. Due to the non-adiabatic transitions, in general, our prepared state at time t_1 is not an energy eigenstate but a superposition state of the energy eigenstates. Similarly

the non-adiabatic transition also occurs from $t_1 + \tau$ to $2t_1 + \tau$. We will explain that these non-adiabatic transitions cause high frequency oscillations in our scheme.

At the step 3, we prepare a state $|\psi(0)\rangle$, let this state by the Hamiltonian for a time t , and we obtain $|\psi(t)\rangle$. We perform a unitary evolution at the step 4, and we perform a projective measurement on the state at the step 5. If we combine the step 4 and 5, this process corresponds to a projective measurement $|\phi(t)\rangle\langle\phi(t)|$ on the state $|\psi(t)\rangle$.

An overlap between states should be $\langle\phi(t)|\psi(t)\rangle = \langle\tilde{\phi}(t)|\tilde{\psi}(t)\rangle$ where we define

$$\langle\tilde{\phi}(t)| = \langle\phi(t)|e^{-ist\mathcal{H}_{\text{QA}}}. \quad (\text{B9})$$

Using the rotating wave approximation, the final transition amplitude is calculated as

$$\begin{aligned} \langle\tilde{\phi}(t)|\tilde{\psi}(t)\rangle &= \langle\tilde{\phi}(t)|e^{-it\mathcal{H}_{\text{eff}}}|\tilde{\psi}(0)\rangle, \\ &= \langle\phi(t)|e^{-ist\mathcal{H}_{\text{QA}}}e^{-it\mathcal{H}_{\text{eff}}}|\psi(0)\rangle, \end{aligned} \quad (\text{B10})$$

where we use the effective Hamiltonian described in the Eq. (19). Since we prepare a superposition of different energy eigenstates by a nonadiabatic transition and then perform a projective measurement into another superposition of energy eigenstates, the difference between the energy eigenvalues should affect the oscillation. We will show this point below.

Let us assume that we are only interested in two states $|k\rangle$ and $|l\rangle$. In this case, we can approximate the Hamiltonian as $\mathcal{H}_{\text{QA}} \simeq \frac{\Delta}{2}\sigma_z = |l\rangle\langle l| - |k\rangle\langle k|$. Also, we can use the Eq. (B2) for the effective Hamiltonian. The transition amplitude (B10) is calculated as

$$\begin{aligned} \langle\phi(t)|e^{-ist\frac{\Delta}{2}\sigma_z}e^{-it\mathcal{H}_{\text{eff}}}|\psi(0)\rangle &= \cos\frac{\tilde{\lambda}'}{2}t\langle\phi(t)|e^{-ist\frac{\Delta}{2}\sigma_z}|\psi(0)\rangle - i\sin\frac{\tilde{\lambda}'}{2}t\langle\phi(t)|e^{-ist\frac{\Delta}{2}\sigma_z}U_{\text{diag}}^\dagger\sigma_x U_{\text{diag}}|\psi(0)\rangle, \\ &= \cos\frac{\tilde{\lambda}'}{2}t\left(\langle\phi(t)|l\rangle\langle l|\psi(0)\rangle e^{-ist\frac{\Delta}{2}} + \langle\phi(t)|k\rangle\langle k|\psi(0)\rangle e^{ist\frac{\Delta}{2}}\right) \\ &\quad - i\sin\frac{\tilde{\lambda}'}{2}t\left(\langle\phi(t)|l\rangle\langle l|U_{\text{diag}}^\dagger\sigma_x U_{\text{diag}}|\psi(0)\rangle e^{-ist\frac{\Delta}{2}} + \langle\phi(t)|k\rangle\langle k|U_{\text{diag}}^\dagger\sigma_x U_{\text{diag}}|\psi(0)\rangle e^{ist\frac{\Delta}{2}}\right). \end{aligned} \quad (\text{B11})$$

We can see that the absolute square of (B11) includes 5 different frequency modes,

$$\begin{aligned} \Omega &= 0, \tilde{\lambda}', s\Delta - \tilde{\lambda}', s\Delta, s\Delta + \tilde{\lambda}'. \\ &= 0, \tilde{\lambda}', \omega - \tilde{\lambda}', \omega, \omega + \tilde{\lambda}'. \end{aligned} \quad (\text{B12})$$

Although we have 5 peaks, it is easy to specify the target peak for the following reason. As we mentioned in the main text, we sweep the frequency range of $0 < \Omega \ll \omega$, and so we only observe a peak $\tilde{\lambda}'$.

Appendix C: Results for strong non-adiabatic transitions

In the main text, we consider a case that the non-adiabatic transition is not relevant. In this section, we investigate the performance of our scheme when we increase the effect of the non-adiabatic transitions in case E .

We plot the spectrum by setting $T_{\text{ann}} = 3$ and $t_1/T_{\text{ann}} = 0.9$, in Fig. 11 (a). Here, as a guide to the eye, we draw a blue line corresponding to the analytical curve of Eq. (22) where we use the actual values of

$|\langle 1|\dot{\mathcal{H}}|0\rangle|$ and $(E_1 - E_0)$, and this is the target peak in the spectrum. We plot the magnified view in Fig. 11 (b).

We observe unexpected peaks at frequencies of around $\Omega = 0.38$ in the spectrum, and this height is more significant than the target peak. So, if we naively adopt our method described in Eq. (33), we obtain wrong estimated values about the transition matrix element and energy gap.

To understand the origin of these unexpected peaks, we perform analytical calculations to obtain resonant frequencies in the spectrum with non-adiabatic transitions in Appendix B 2. Although peaks at $\Omega = \omega - \Omega_{\text{ana}}^{(0,1)}(\omega)$, ω , $\omega + \Omega_{\text{ana}}^{(0,1)}(\omega)$ should exist, we could not observe this due to the restrict range of Ω in the spectrum, as we mentioned in Appendix B 2. On the other hand, if there is a non-negligible population of the second excited state induced by the non-adiabatic transitions, we should observe peaks at frequencies of $\Omega = \omega - \Omega_{\text{ana}}^{(1,2)}(\omega)$, ω , $\omega + \Omega_{\text{ana}}^{(1,2)}(\omega)$. To see these points, we plot the spectrum in the Fig 12, and actually observe such three peaks. Moreover, when ω is far from the energy difference $(E_2 - E_1)$, the peak at a frequency of $\omega - \Omega_{\text{ana}}^{(1,2)}(\omega)$ asymptotically approaches the energy difference $(E_2 - E_1)$, and this is the origin of the highest peaks in Fig 11(a). The frequency of $\omega - \Omega_{\text{ana}}^{(1,2)}(\omega)$ is much smaller than $\omega - \Omega_{\text{ana}}^{(0,1)}(\omega)$, ω , $\omega + \Omega_{\text{ana}}^{(0,1)}(\omega)$, and so we unfortunately observe this peak even if we restrict the range of Ω in the spectrum.

Even when we observe these peaks other than target peaks, there is a way to estimate the transition matrix element and energy gap. As we mentioned in the main text (in sec. IV C 2), we have a modified method to identify the target peak, which is useful for this case as well. The positions of the target peak are expected to be fitted by the analytical formula in Eq. (22). This means that, if we fail to fit the peaks, we can guess that such peaks do not correspond to the peak from the Rabi oscillation. Indeed, the peak $\Omega \simeq 0.38$ cannot be fitted by the equation Eq. (22) well. On the other hand, if we focus on the peaks with frequencies of around $\Omega = 0.01$, as shown in Fig. 11 (b), we can fit these peaks by the analytical formula, and so we can accurately estimate the transition matrix element and energy gap.

Also, we plot the spectrum by setting $T_{\text{ann}} = 3$ and $t_1/T_{\text{ann}} = 0.7$, in Fig. 13 (a). Here, as a guide to the eye, we draw a yellow line corresponding to the analytical curve of Eq. (22), which are the target peaks. Here, not only the target peaks but also other peaks are observed. These come from the higher order perturbation, which can be observed for a larger Rabi frequency (see the appendix D). Fortunately, we can distinguish these secondary peak from the target peaks as follows.

First, the secondary peaks are usually smaller than the target peaks. In Fig. 13, except a few points, the target peaks are the highest in this frequency region. Second, from the fitting results by the Eq. (22), we can distinguish the target peaks from the secondary peaks (For example,

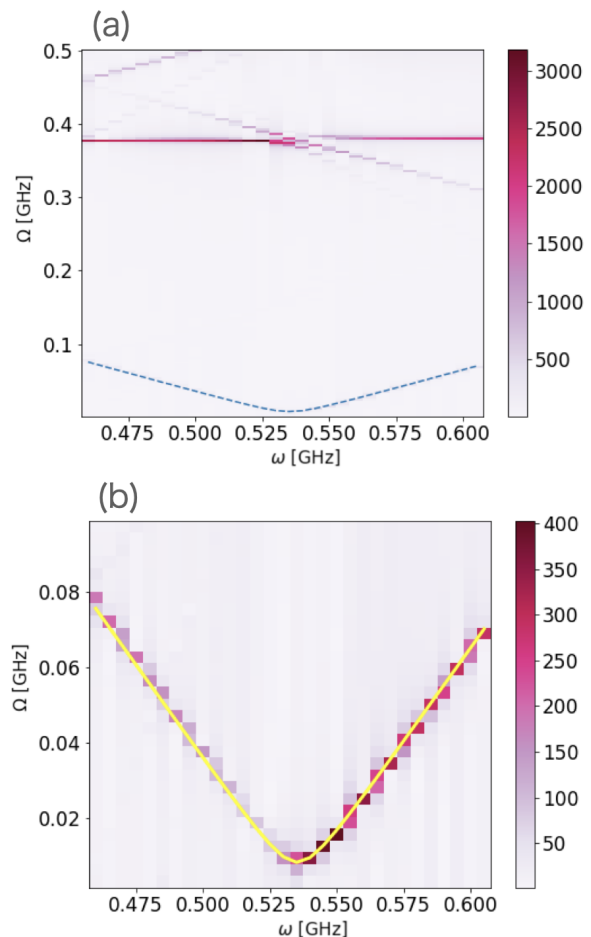


FIG. 11. In case E, we plot the power spectrum $P(\omega, \Omega)$ where we set $T_{\text{ann}} = 3$ and $t_1/T_{\text{ann}} = 0.9$ in (a). Also, we plot the magnified view in (b). The blue and yellow lines are the target peaks obtained by diagonalization. The peak we want is seen at the correct position when Ω is enlarged in the small region, but it is lower than the high-frequency peak around $\Omega = 0.38$.

the slope of the target peaks are given as $\frac{d\Omega_{\text{ana}}(\omega)}{d\omega} \simeq 1$ for a large ω , while the slope of the secondary peaks are twice larger than this.) Third, the λ dependence of the peak height is different. The height of the target peaks scales as λ^2 while that of the secondary peak scale as λ^4 , and this let us know which is the target peak by sweeping λ . Actually, in Fig. 13, we plot the spectrum by choosing a smaller λ , and show that the secondary peak becomes almost invisible compared to the target peak.

Appendix D: Perturbative approach of this method

In the main text, we used the RWA and the Hamiltonian effectively transformed to simple two-dimensional one. When we consider the higher-order perturbation, there can be other peaks without the $|E_1 - E_0| = \omega$ condition.

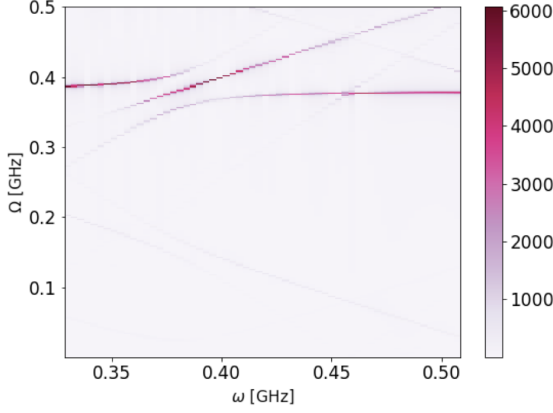


FIG. 12. Plot of the spectrum to focus the peak due to a transition from the first excited state to the second excited state, in case E. We observe three peaks around $\Omega \simeq \omega \simeq 0.38$. These correspond to frequencies of $\Omega = \omega - \Omega_{\text{ana}}^{(1,2)}(\omega)$, ω , $\omega + \Omega_{\text{ana}}^{(1,2)}(\omega)$.

We calculate the transition amplitude $\langle f|U(t,0)|i\rangle$, where $U(t,0)$ is a unitary operator expressing the time evolution from time 0 to time t , $|i\rangle$ and $|f\rangle$ are the initial state and the final state respectively.

First, we describe the Hamiltonian of Eq. (7) in the so-called interaction picture

$$\tilde{\mathcal{H}}(t) = \lambda e^{it\mathcal{H}_{\text{QA}}} \dot{\mathcal{H}} e^{-it\mathcal{H}_{\text{QA}}} \cos \omega t. \quad (\text{D1})$$

Then, the transition amplitude is given by

$$\begin{aligned} \langle f|U(t,0)|i\rangle &= \langle f|\tilde{i}\rangle + (-i) \int_0^t d\tau \langle \tilde{f}|\tilde{\mathcal{H}}(\tau)|\tilde{i}\rangle \\ &+ (-i)^2 \int_0^t d\tau_1 \int_0^{\tau_1} d\tau_2 \langle \tilde{f}|\tilde{\mathcal{H}}(\tau_1)\tilde{\mathcal{H}}(\tau_2)|\tilde{i}\rangle + \dots, \end{aligned} \quad (\text{D2})$$

where the tilde symbol means that the states are in the interaction picture. Since the Schrodinger picture coincides with the interaction picture at $t = 0$, we have $|\tilde{i}\rangle = |i\rangle$. We assume that λ is small, and will calculate the transition amplitude up to the second order of the perturbation theory.

In our method, we assume that the dynamics are adiabatic in the second and fourth steps. In this case, we can set $|i\rangle = |0\rangle$ and $|f\rangle = |m\rangle$, and we will evaluate the quantity of $p_{0,m}(t) = |\langle m|U(t,0)|0\rangle|^2$.

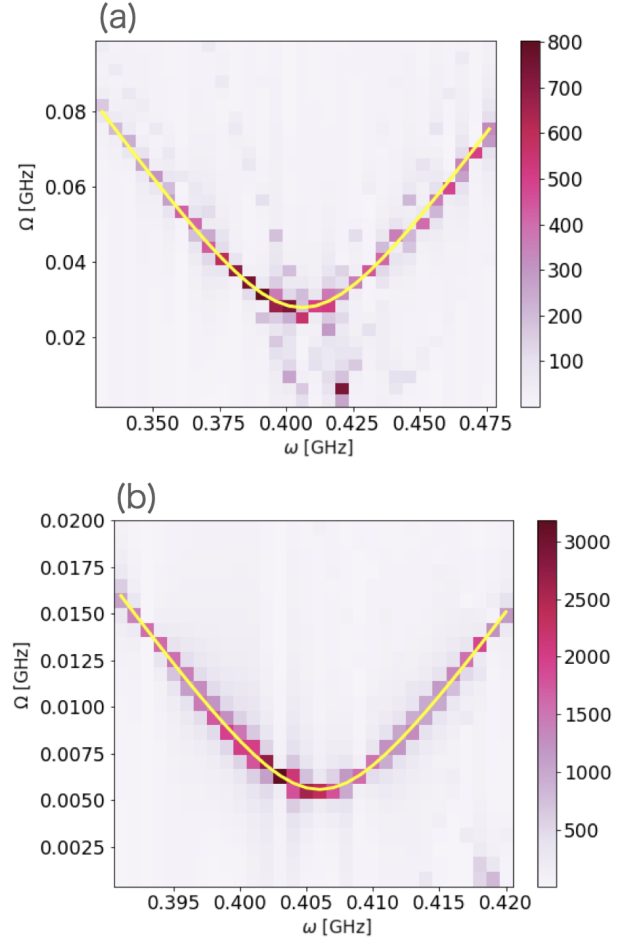


FIG. 13. Plot of the power spectrum in case E with $T_{\text{ann}} = 3$ and $t_1/T_{\text{ann}} = 0.7$. Here, as a guide to the eye, we draw a yellow line corresponding to the analytical curve of Eq. (22), which are the target peaks. (a) We choose $\lambda/T_{\text{ann}} = 0.05$. We observe not only the target peaks but also the peaks due to the higher order perturbation. (b) We choose $\lambda/T_{\text{ann}} = 0.01$. Compared to the case with $\lambda/T_{\text{ann}} = 0.05$, the peaks caused by higher-order perturbations are smaller.

1. First-order perturbation and the Rabi oscillation

Let us consider the first order of the perturbative term in Eq. (D2) as follows.

$$\begin{aligned} & \int_0^t d\tau \langle \tilde{m}|\tilde{\mathcal{H}}(\tau)|\tilde{0}\rangle \\ &= \lambda \int_0^t d\tau \langle m|e^{-it\mathcal{H}_{\text{QA}}} e^{i\tau\mathcal{H}_{\text{QA}}} \dot{\mathcal{H}} e^{-i\tau\mathcal{H}_{\text{QA}}} |0\rangle \cos \omega \tau \\ &= \lambda \langle m|\dot{\mathcal{H}}|0\rangle \int_0^t d\tau e^{-iE_m t + i(E_m - E_0)\tau} \cos \omega \tau \\ &= \frac{\lambda}{2} \langle m|\dot{\mathcal{H}}|0\rangle e^{-iE_m t} \\ & \quad \cdot \left(\frac{e^{i(E_m - E_0 + \omega)t} - 1}{i(E_m - E_0 + \omega)} + \frac{e^{i(E_m - E_0 - \omega)t} - 1}{i(E_m - E_0 - \omega)} \right). \end{aligned} \quad (\text{D3})$$

The absolute square of (D3) includes terms with frequencies of 2ω , $E_m - E_0 \pm \omega$. This result is consistent with the analytical result in Eq. (22) in the limit of small λ , which predicts a resonance at $\Omega = |E_m - E_0 - \omega|$.

2. Second-order perturbation

Let us consider three energy eigenstates of \mathcal{H}_{QA} as $|0\rangle$, $|I\rangle$, $|m\rangle$ and we assume $|i\rangle = |0\rangle$ and $|f\rangle = |m\rangle$. The third term of the r.h.s. of (D2) is

$$(-i)^2 \lambda^2 \int_0^t dt_1 \int_0^{t_1} dt_2 \sum_i \langle m | \dot{\mathcal{H}} | i \rangle \langle i | \dot{\mathcal{H}} | 0 \rangle e^{-iE_m t + i(E_m - E_i)t_1} \cdot e^{i(E_i - E_0)t_2} \cos \omega t_1 \cos \omega t_2, \quad (\text{D4})$$

$$= (-i)^2 \lambda^2 \langle m | \dot{\mathcal{H}} | I \rangle \langle I | \dot{\mathcal{H}} | 0 \rangle \frac{e^{i(E_m - E_0 - 2\omega)t} - 1}{(E_I - E_0 - \omega)(E_m - E_0 - 2\omega)} + \dots \quad (\text{D5})$$

The absolute square of this amplitude includes various modes, but one of them is $E_m - E_0 - 2\omega$. This means that the probability function $p_{0,m}(\tau)$ includes an oscillation with a frequency of $\Omega = 2(\omega - (E_m - E_0)/2)$. Importantly, for this frequency, we have $\frac{d\Omega}{d\omega} = 2$, while we have $\frac{d\Omega_{\text{anna}}}{d\omega} = 1$ for our analytical formula in Eq. (22).

-
- [1] P. Ehrenfest, Adiabatische invarianten und quantentheorie, *Annalen der Physik* **356**, 327 (1916).
- [2] T. Kato, On the adiabatic theorem of quantum mechanics, *Journal of the Physical Society of Japan* **5**, 435 (1950).
- [3] M. Amin, Consistency of the adiabatic theorem, *Physical Review Letters* **102**, 220401 (2009).
- [4] A. Dodin and P. Brumer, Generalized adiabatic theorems: Quantum systems driven by modulated time-varying fields, *PRX Quantum* **2**, 030302 (2021).
- [5] B. Apolloni, C. Carvalho, and D. de Falco, Quantum stochastic optimization, *Stochastic Processes and their Applications* **33**, 233 (1989).
- [6] T. Kadowaki and H. Nishimori, Quantum annealing in the transverse ising model, *Physical Review. E* **58**, 5355 (1998).
- [7] E. Farhi, J. Goldstone, S. Gutmann, and M. Sipser, Quantum computation by adiabatic evolution, arXiv preprint [10.48550/arXiv.quant-ph/0001106](https://arxiv.org/abs/10.48550/arXiv.quant-ph/0001106) (2000).
- [8] R. D. Somma, D. Nagaj, and M. Kieferová, Quantum speedup by quantum annealing, *Phys. Rev. Lett.* **109**, 050501 (2012).
- [9] S. Muthukrishnan, T. Albash, and D. A. Lidar, Tunneling and speedup in quantum optimization for permutation-symmetric problems, *Phys. Rev. X* **6**, 031010 (2016).
- [10] M. B. Hastings, The Power of Adiabatic Quantum Computation with No Sign Problem, *Quantum* **5**, 597 (2021).
- [11] T. Imoto, Y. Seki, and Y. Matsuzaki, Obtaining ground states of the xxz model using the quantum annealing with inductively coupled superconducting flux qubits, *Journal of the Physical Society of Japan* **91**, 064004 (2022).
- [12] R. Miyazaki, Effective spin models of kerr-nonlinear parametric oscillators for quantum annealing, *Phys. Rev. A* **105**, 062457 (2022).
- [13] J. Roland and N. J. Cerf, Quantum search by local adiabatic evolution, *Phys. Rev. A* **65**, 042308 (2002).
- [14] C. C. Chang, K. S. McElvain, E. Rrapaj, and Y. Wu, Improving schrödinger equation implementations with gray code for adiabatic quantum computers, *PRX Quantum* **3**, 020356 (2022).
- [15] B. F. Schiffer, J. Tura, and J. I. Cirac, Adiabatic spectroscopy and a variational quantum adiabatic algorithm, *PRX Quantum* **3**, 020347 (2022).
- [16] R. Babbush, P. J. Love, and A. Aspuru-Guzik, Adiabatic quantum simulation of quantum chemistry, *Scientific Reports* **4** (2014).
- [17] A. Teplukhin, B. K. Kendrick, S. Tretiak, and P. A. Dub, Electronic structure with direct diagonalization on a d-wave quantum annealer, *Scientific Reports* **10**, [10.1038/s41598-020-77315-4](https://doi.org/10.1038/s41598-020-77315-4) (2020).
- [18] M. Benedetti, J. Realpe-Gómez, R. Biswas, and A. Perdomo-Ortiz, Quantum-assisted learning of hardware-embedded probabilistic graphical models, *Physical Review X* **7**, 041052 (2017).
- [19] P. Date and T. Potok, Adiabatic quantum linear regression, *Scientific Reports* **11**, [10.1038/s41598-021-01445-6](https://doi.org/10.1038/s41598-021-01445-6) (2021).
- [20] A. Mott, J. Job, J.-R. Vlimant, D. Lidar, and M. Spiropulu, Solving a higgs optimization problem with quantum annealing for machine learning, *Nature* **550** (2017).
- [21] A. M. Childs, E. Farhi, and J. Preskill, Robustness of adiabatic quantum computation, *Phys. Rev. A* **65**, 012322 (2001).
- [22] S. Morita and H. Nishimori, Mathematical foundation of quantum annealing, *Journal of Mathematical Physics* **49**, [125210](https://doi.org/10.1063/1.2995837) (2008), <https://doi.org/10.1063/1.2995837>.
- [23] T. Albash and D. A. Lidar, Adiabatic quantum computation, *Reviews of Modern Physics* **90**, 015002 (2018).
- [24] P. Hauke, H. G. Katzgrabe, W. Lechner, H. Nishimori, and W. D. Oliver, Perspectives of quantum annealing: methods and implementations, *Reports on Progress in Physics* **83**, 054401 (2020).
- [25] Y. Matsuzaki, H. Hakoshima, K. Sugisaki, Y. Seki, and S. Kawabata, Direct estimation of the energy gap between the ground state and excited state with quantum annealing, *Japanese Journal of Applied Physics* **60**,

- SBBI02 (2021).
- [26] A. E. Russo, K. M. Rudinger, B. C. Morrison, and A. D. Baczewski, Evaluating energy differences on a quantum computer with robust phase estimation, *Physical Review Letters* **126**, 210501 (2021).
- [27] R. Bialczak, M. Ansmann, M. Hofheinz, M. Lenander, E. Lucero, M. Neeley, A. O’Connell, D. Sank, H. Wang, M. Weides, *et al.*, Fast tunable coupler for superconducting qubits, *Physical Review Letters* **106**, 060501 (2011).
- [28] D. Zeuch, F. Hassler, J. J. Slim, and D. P. DiVincenzo, Exact rotating wave approximation, *Annals of Physics* **423**, 168327 (2020).
- [29] K. Konishi and G. Paffuti, *Quantum Mechanics: A New Introduction* (Oxford University Press, 2009).
- [30] D-wave, *Qpu solver datasheet* (2017).
- [31] D. Manzano, A short introduction to the lindblad master equation, *AIP Advances* **10**, 025106 (2020).
- [32] F. Yoshihara, K. Harrabi, A. Niskanen, Y. Nakamura, and J. S. Tsai, Decoherence of flux qubits due to $1/f$ flux noise, *Physical review letters* **97**, 167001 (2006).
- [33] T. Jörg, F. Krzakala, J. Kurchan, A. C. Maggs, and J. Pujos, Energy gaps in quantum first-order mean-field-like transitions: The problems that quantum annealing cannot solve, *EPL (Europhysics Letters)* **89**, 40004 (2010).
- [34] Y. Seki, S. Tanaka, and S. Kawabata, Quantum phase transition in fully connected quantum wajnflasz-pick model, *Journal of the Physical Society of Japan* **88**, 054006 (2019).
- [35] S. Watabe, Y. Seki, and S. Kawabata, Enhancing quantum annealing performance by a degenerate two-level system, *Scientific Reports* **10**, 10.1038/s41598-019-56758-4 (2020).
- [36] J. R. Johansson, P. Nation, and F. Nori, Qutip 2: A python framework for the dynamics of open quantum systems, *Computer Physics Communications* **184**, 1234 (2013).